JOURNAL OF MATERIALS SCIENCE 28 (1993) 3089–3096

Effect of laser surface melting on the corrosion resistance of chromium-plated 9Cr–1Mo ferritic steel in an acidic medium

M. G. PUJAR, R. K. DAYAL, A. S. KHANNA*
Metallurgy Division, Indira Gandhi Centre for Atomic Research, Kalpakkam 603 102, India
E. W. KREUTZ
Fraunhofer Institute for Lasertechnik, Aachen, Germany

9Cr–1Mo ferritic steel forms an integral part of some of the nuclear power generating industries where it is used as the steam generating material. Its corrosion resistance could be further improved by employing a chromium coating over it. However, this chromium coating has been found to be unsatisfactory owing to the microcracks present in the coating. Laser surface melting (LSM) could be effectively used not only to remove these microcracks but also to form a better corrosion-resistant modified surface without affecting the bulk properties of the material. Studies were carried out on the laser surface melted chromium-plated 9Cr–1Mo steel. The specimens with chromium deposit thicknesses ranging from 30–70 μm were prepared and then laser irradiated. Optical microscopic studies on the cross-sections of these specimens revealed an average laser-melted thickness of around 0.1–0.5 mm, depending upon the irradiation parameter used. Aqueous corrosion behaviour of these specimens was studied by anodic polarization in 1N H_2SO_4 medium. Anodic polarization experiments were carried out for specimens after repolishing the same specimen until the 9Cr–1Mo base metal was reached. The passive and peak current density values, range of passivity, peak and transpassive potentials, were determined at each stage of polishing, and these were compared with those of pure chromium metal as well as 9Cr–1Mo alloy in the same medium. Observation of these data indicates that the laser surface melting could be beneficial in raising the aqueous corrosion resistance of such chromium-coated steels, to a level comparable with that of the pure chromium metal.

1. Introduction

Laser surface alloying is hailed as the latest technique whereby a desired alloy composition can be achieved *in situ* on a workpiece surface with the help of laser-beam heating. This technique enables one to use a surface of a less expensive workpiece and locally modify it by imparting properties corresponding to high-performance alloys. Attainment of extremely high temperatures due to the laser-beam heating together with the addition of alloying elements in the form of powder or thin coating, result in the localized melting of the substrate to form an entirely different surface having a different microstructure. This kind of surface modification is being tried for improved corrosion and wear-resistance purposes, while retaining the original properties of the bulk. In the recent past, there have been many examples showing the importance of laser surface melting and alloying to improve substrate properties [1–10]. It is reported that, good intergranular corrosion resistance could be obtained by laser surface treatment of the sensitized stainless steel [8, 9, 11]. This has been attributed to the formation of a thin barrier of unsensitized material due to laser irradiation between the corrosive environment and the underlying sensitized microstructure [12]. It has also been reported [8] that the laser surface melting (LSM) technique could be used *in situ* to modify the microstructure of already sensitized 316 ss, in order to improve the localized corrosion resistance of such materials in the as-received, as well as in the cold-worked, conditions. This technique has been found [10] to be useful in increasing pitting resistance of the 316 ss materials. Ion *et al.* [13] have demonstrated through their work on 13.5% Cr and 0.6% C that, the laser surface melting could dissolve the carbides, homogenize the alloying elements and produce martensite through self quenching, the process being cost effective and on par with the conventional heat treatments. They also showed that laser-melting of samples at higher traverse rates led to the less preferential pitting. It has also been experimentally proved that laser surface melting could reduce cavitation erosion corrosion [14].

The chromium–molybdenum steels are extensively

Present address: Indian Institute of Technology, Bombay, India.

0022–2461

TABLE I Chemical composition of 9Cr–1Mo steel

	C	Si	Mn	S	P	Cr	Mo	Fe
wt %	0.09	0.75	0.67	0.003	0.02	9.27	1.05	Bal.

TABLE II Laser processing parameters

Specimen	Type of laser	Laser power (kW)	Speed (mm min^{-1})	Shielding gas
CO1	CW CO2	3.0	500	Argon
CO2	CW CO2	3.0	500	Argon
CO3	CW CO2	3.0	250	Argon
ND1	Nd-YAG (pulsed)	[a]	500	Nitrogen
ND2	Nd-YAG (pulsed)	[a]	500	Nitrogen

[a] Repetition rate 80 Hz, pulse length 4 ms, pulse energy 5 J.

used in power-generating industries due to their high strength at elevated temperatures. Amongst these, 2.25Cr–1Mo and 9Cr–1Mo steels are widely used. 2.25Cr–1Mo ferritic steel is known for its inadequate aqueous corrosion resistance compared to 9Cr–1Mo ferritic steels. The corrosion resistance of these materials is dependent on the environmental factors, namely pressure and moisture content [15]. Because it is already established [16] that the passive film formed on these steels in an acidic medium is composed of the loose corrosion deposits and is unstable, it is possible to protect the surfaces of these materials by electroplating them with chromium metal. However, such chromium deposits contain microcracks through which the aqueous solution in that vicinity can reach the base metal; hence to overcome this problem laser surface melting treatment could be adopted. The laser surface melting not only removes these microcracks, but also helps in forming a uniform, crack- and pore-free surface. The LSM zone so formed has a chemical composition which is altogether different from that of the base metal and it becomes important to know the corrosion resistance of such laser-treated material across its LSM zone. This paper discusses the aqueous corrosion resistance of laser-melted chromium-coated 9Cr–1Mo ferritic steel surface. A potentiodynamic anodic polarization technique was used to study the relative corrosion resistance of the laser-melted surfaces of the 9Cr–1Mo alloy.

2. Experimental procedure

2.1. Electroplating of chromium on 9Cr–1Mo alloy

Electroplating of chromium was carried out on circular (25 mm diameter, 5 mm thick) specimens of 9Cr–1Mo ferritic steel, the chemical composition of which is given in Table I, by using a conventional electrochemical bath of chromic acid and sulphuric acid. The details of the plating procedure are mentioned elsewhere [17]. Average chromium deposit thickness was calculated using the initial dimensions of the specimens and the weight gain after plating.

2.2. Laser surface melting

Specimens designated CO1, CO2 and CO3 were surface melted by using a continuous wave (CW) CO2 laser at a power of 3 kW. Specimens designated ND1 and ND2 were surface melted by using pulsed Nd–YAG laser with an average pulse energy of 5 J. The details of the laser-irradiation parameters of these specimens are given in Table II.

TABLE III Characteristics of the LSM and HAZ zones for different specimens

Specimen	Chromium deposit thickness (μm)	LSM zone thickness (μm)	HAZ width (μm)
CO1	71	141	269
CO2	29	377	1023
CO3	62	142	280
ND1	31	494	565
ND2	78	412	569

2.3. Optical microscopic studies

The laser-irradiated specimens were cut into semi-circular pieces. One part was mounted in epoxy resin such that the cross-section of the specimen was exposed. These mounted specimens were polished up to fine-diamond grit, cleaned and electrolytically etched in 10% chromic acid to reveal the laser surface melted (LSM) zone. Optical microscopic observations of these cross-sections were carried out to calculate the LSM and heat-affected zone (HAZ) thickness values. The optical microscopic observations, together with the chromium deposit values, are presented in Table III.

2.4. Corrosion-resistance studies

The laser-melted and cut specimens were mounted in epoxy resin for electrochemical studies such that the irradiated surface was exposed to the electrolyte. Anodic polarization experiments were carried out in 0.5 M H_2SO_4, which was deaerated by bubbling oxygen-free pure hydrogen gas through it during the experimentation. All the electrode potential measurements were

carried out with respect to a saturated calomel electrode (SCE) and the potential scan rate was maintained at 10 mV min^{-1}. The anodic polarization experiments were started from a cathodic potential of − 600 mV (SCE) and were continued until transpassivity was attained. All the potentiodynamic anodic polarization experiments were carried out after repolishing the same specimen up to 600 grit until the 9Cr–1Mo base metal was reached, in order to determine the effect of different LSM layers. The thickness of the layer removed during every polishing stage was approximately calculated to be 20 μm. Similar polishing of these specimens at lower grit (220) for a specific time period was found to reduce the thickness of the LSM zone by around 80 μm. Anodic polarization curves thus obtained at every stage were further analysed to tabulate the passive current and peak current density values, as well as the range of passivation. The peak potential and transpassive potential values were also obtained for every stage. The data points obtained for all these parameters were plotted against the LSM zone thickness. Polarization curves for untreated 9Cr–1Mo alloy and pure chromium metal were also obtained in this medium and analysed for their corrosion behaviour.

3. Results and discussion

3.1. Characterization of the LSM zone

The melting temperatures involved during laser material processing are extremely high. Attainment of such high temperatures coupled with the very high cooling rates of the order of 10^7 K s^{-1} result in metastable microstructure. Such heat-treatment conditions result in the resolidification of the melted zone in an epitaxial fashion [18]. This is evident in the photomicrographs for specimens CO1, CO2 and CO3 (Figs 1–3). The fine dendritic microstructure that is observed in specimen CO3, compared to the microstructure of specimen CO1 having large elongated grains, is attributed to the different interaction time of the laser beam with the substrate surface. The interaction time of the laser beam with specimen CO3 is double that of specimen CO1 (see Table II, travel speed of the beam). The higher temperature gradient reached in specimen CO3, together with the higher solidification rate, leads to the formation of the fine dendritic type of microstructure [19]. The specimens irradiated with a pulsed Nd–YAG laser beam showed (Figs 4 and 5) a dual-phased microstructure which was well resolved. During laser irradiation of a coated specimen, the coating as well as part of the substrate beneath it is melted. The constituent elements forming the substrate get mixed up with the elements of the molten coating. Finally the LSM zone has a chemical composition which is different from that of the substrate alloy, as modelled by Draper [1]. Based on this principle, and assuming negligible evaporation losses of deposited chromium during laser melting, the average chemical composition of all the specimens was calculated. These values of chemical composition have been presented in Table IV.

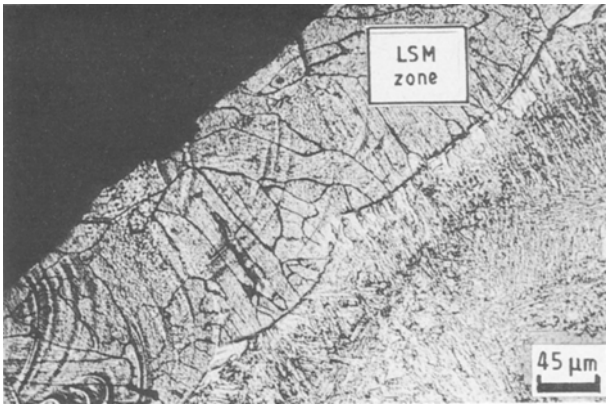

Figure 1 Cross-section of LSM zone for specimen CO1. Electrochemically etched in 10% chromic acid.

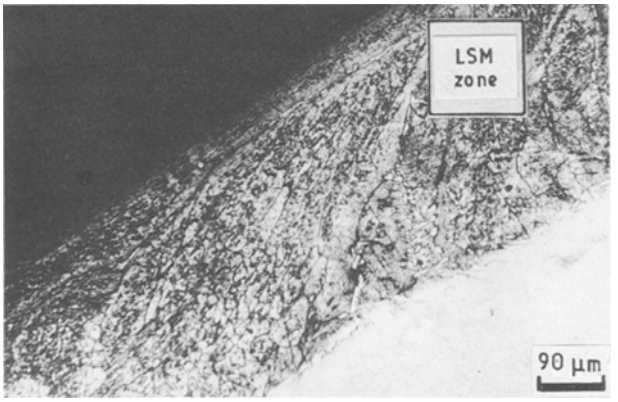

Figure 2 Cross-section of LSM zone for specimen CO2. Electrochemically etched in 10% chromic acid.

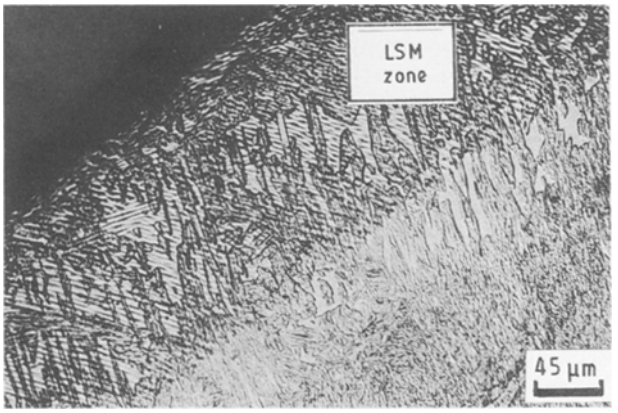

Figure 3 Cross-section of LSM zone for specimen CO3. Electrochemically etched in 10% chromic acid.

3.2. Corrosion studies in an acidic medium

It has been observed by some workers [20, 21], that even helium gas protection during laser surface treatment was not enough to prevent the oxidation of the as-processed surface of the materials. Because this oxide film formed is a few nanometres thick, the earlier workers [5] used the method of cathodic cleaning of the as-processed surfaces in 1 N H_2SO_4 at − 0.5 V or − 1.0 V (SCE) for 5–15 min. However, it has been reported [22] that the native oxide film present on the

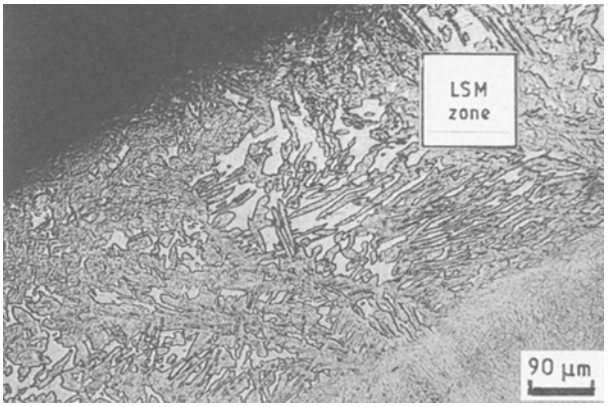

Figure 4 Cross-section of LSM zone for specimen ND1. Electrochemically etched in 10% chromic acid.

Figure 5 Cross-section of LSM zone for specimen ND2. Electrochemically etched in 10% chromic acid.

TABLE IV Chemical composition of LSM zones of different specimens based on calculations

Specimen	Cr (wt %)	Fe (wt %)	Mo (wt %)
CO1	54.90	44.60	0.50
CO2	16.72	82.36	0.92
CO3	49.27	50.17	0.56
ND1	16.49	82.57	0.94
ND2	26.87	72.32	0.81

Taking the density of 9Cr–1Mo = 7.83 $g cm^{-3}$, and of chromium metal = 7.19 $g cm^{-3}$.

as-processed specimens is not reduced by the cathodic treatment used for any length of time. This is also due to the lower conductivity of the oxide which results in the anodic and cathodic currents which remain invariant with respect to time of treatment. Also, the as-processed surfaces generally show surface irregularities, shallow grooves [6] and surfaces roughness due to the melting process [7]. Hence, as-processed surfaces of the specimens were first polished on 600 grit emery paper to remove the oxide layer, as well as surface roughness and irregularities before the initiation of the corrosion experiments. Fig. 6 gives the anodic polarization curves for the specimen CO1 obtained at different LSM zone thickness values. The

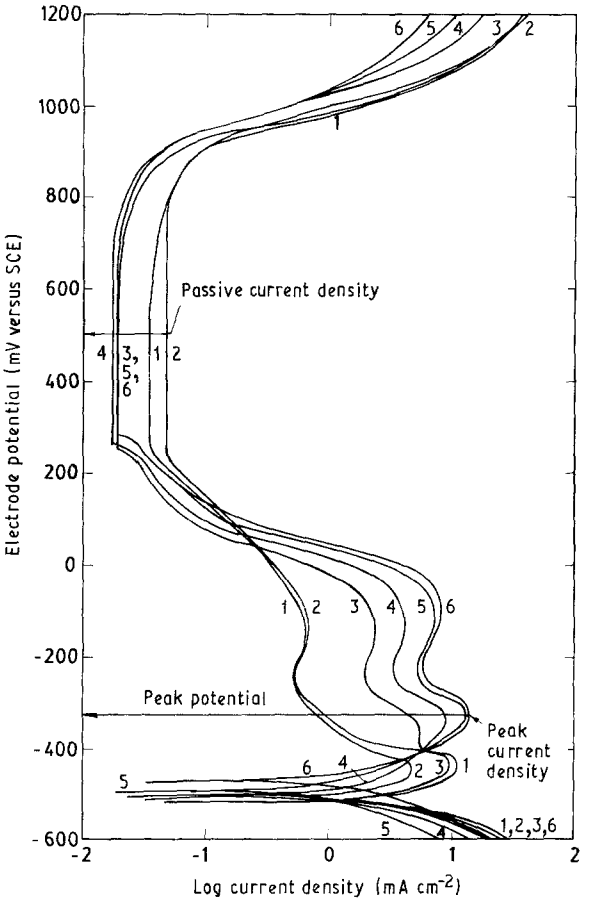

Figure 6 Anodic polarization curves for specimen CO1 obtained at different LSM zone thicknesses in 1N H_2SO_4; 1, 20 μm; 2, 40 μm; 3, 60 μm; 4, 80 μm; 5, 100 μm; 6, 120 μm.

anodic polarization curve of the HAZ of the treated specimens was found to be similar to that of the untreated 9Cr–1Mo alloy.

3.2.1. Passive current density

The passive current density values noted at + 500 mV (SCE) for all the polarization curves were plotted against the LSM zone thickness. The passive current density values of pure chromium metal and 9Cr–1Mo alloy are also indicated for comparison (Figs 7 and 8). It was observed that among specimens CO1, CO2 and CO3, specimen CO1 showed passive current density values as good as pure chromium metal in the bulk of the LSM zone (Fig. 7). In the case of specimen CO2, the values of passive current density in the initial layer of the LSM zone were found to be better than that of 9Cr–1Mo. At the end of the LSM zone the values increased and became comparable to that of 9Cr–1Mo alloy. Specimen CO2 also showed dual-phase microstructure with fine precipitate particles dispersed in the matrix (Fig. 2). The much lower passive current density values observed for specimen CO1 are related to its microstructure (Fig. 1) which is a single-phase large-grained type. Specimen CO3 showed much higher passive current density values initially, which later decreased, but the values were always found to be higher than that for 9Cr–1Mo. It is well known [23] that larger the melting temperature between the substrate and surface material, the worse

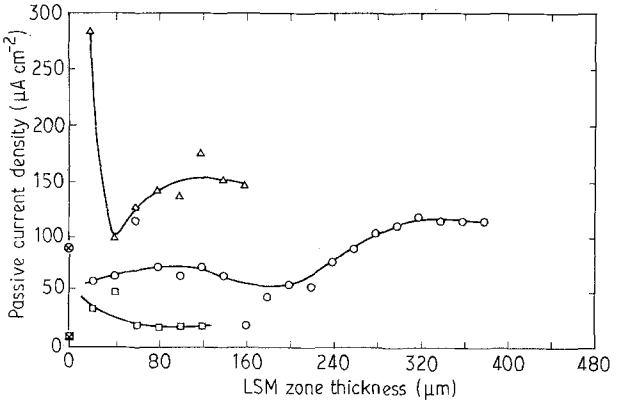

Figure 7 A profile of passive current density values as a function of LSM zone thickness obtained in 1N H_2SO_4. (⊠) Chromium metal, (⊗) 9Cr–1Mo alloy, (□) CO1, (○) CO2, (△) CO3.

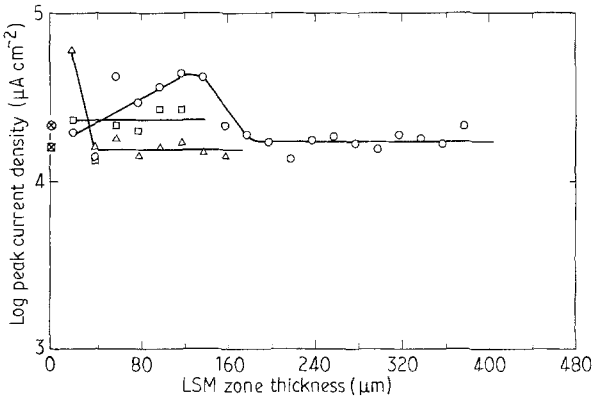

Figure 9 A profile of peak current density values as a function of LSM zone thickness obtained in 1N H_2SO_4. (⊠) Chromium metal, (⊗) 9Cr–1Mo alloy, (□) CO1, (○) CO2, (△) CO3.

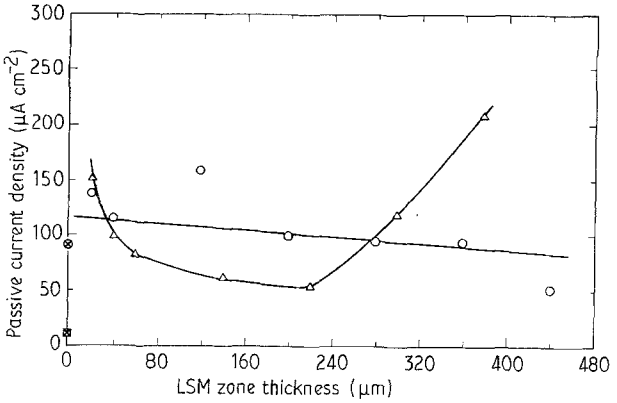

Figure 8 A profile of passive current density values as a function of LSM zone thickness obtained in 1N H_2SO_4. (⊠) Chromium metal, (⊗) 9Cr–1Mo, (△) ND1, (○) ND2.

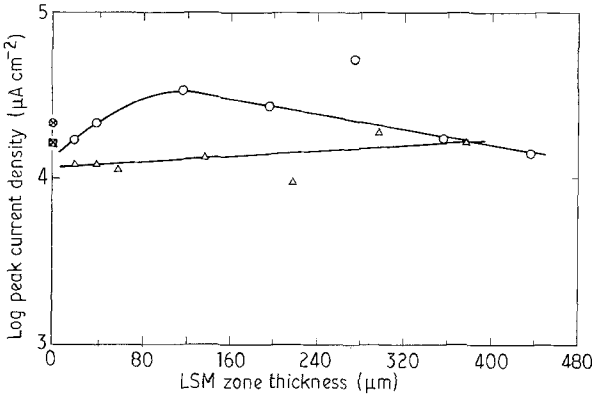

Figure 10 A profile of peak current density values as a function of LSM zone thickness obtained in 1N H_2SO_4. (⊠) Chromium metal, (⊗) 9Cr–1Mo, (△) ND1, (○) ND2.

the homogenization would be. As stated earlier, due to higher interaction time, higher temperatures are attained in the case of specimen CO3. This accounts for the overall higher passive current density values observed due to inhomogenization. In the cases of specimens ND1 and ND2, the initial values, which were higher than 9Cr–1Mo, later decreased in the case of specimen ND1. Specimen ND2 showed better passive current density values after a certain width of the LSM zone in the bulk. In general, these specimens, except for specimen CO3, had better passivation characteristics.

3.2.2. Peak current density

From Fig. 9, it becomes evident that specimen CO1 shows peak current density values as good as 9Cr–1Mo alloy throughout the LSM zone thickness. Specimen CO2 shows an initial rise in the peak current density values which later level off to the values which are lower than that of 9Cr–1Mo alloy. Specimen CO3 showed peak current density values (except for the first one) that are comparable to the peak current density value of pure chromium metal. This implies that specimen CO3 could easily be passivated in this medium.

Fig. 10 shows the behaviour exhibited by specimens ND1 and ND2. Specimen ND1 showed the values which were lower than pure chromium metal or equivalent to it throughout the LSM zone thickness. Specimen ND2 showed an initial value which was comparable to that of the pure chromium metal. These values showed an increase, and subsequently a continuous decrease is observed. In general, this could be considered to be a good performance of this specimen in H_2SO_4 medium. This indicated that both specimens ND1 and ND2 exhibited easier passivation characteristics.

3.2.3. Range of stable passivity

This is an important parameter in determining the passivation behaviour of an alloy. The range of stable passivity values for specimens CO1, CO2 and CO3 were plotted together with those of pure chromium metal and 9Cr–1Mo alloy (Fig. 11). It was observed that specimens CO1 and CO3 showed almost a constant value throughout the LSM zone thickness. But the values exhibited by specimen CO1 were much inferior to that of 9Cr–1Mo alloy, whereas the values exhibited by specimen CO3 were better than 9Cr–1Mo alloy. Specimen CO2 showed a very low initial range of passivity which later gradually increased. Fig. 12 shows the range of passivity for specimens ND1 and ND2. Specimen ND1 exhibited values which were lower than that of the 9Cr–1Mo

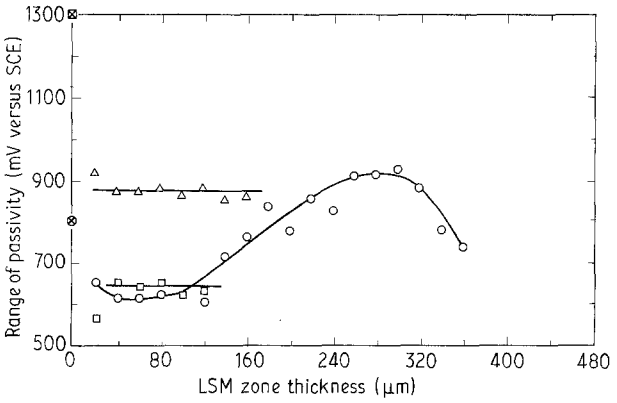

Figure 11 A profile of range of passivity values as a function of LSM zone thickness obtained in 1N H_2SO_4. (⊠) Chromium metal, (⊗) 9Cr–1Mo alloy, (□) CO1, (○) CO2, (△) CO3.

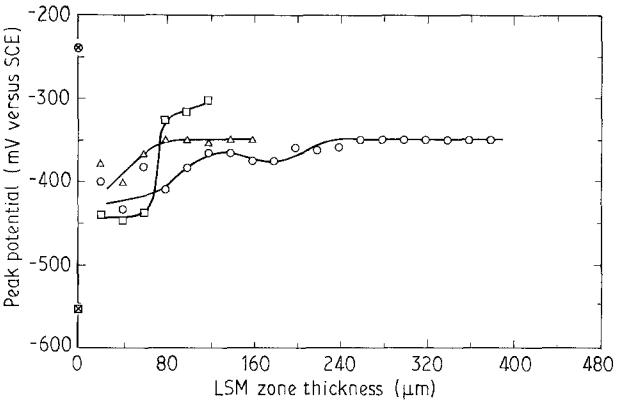

Figure 13 A profile of peak potential values as a function of LSM zone thickness obtained in 1N H_2SO_4. (⊠) Chromium metal, (⊗) 9Cr–1Mo alloy, (□) CO1, (○) CO2, (△) CO3.

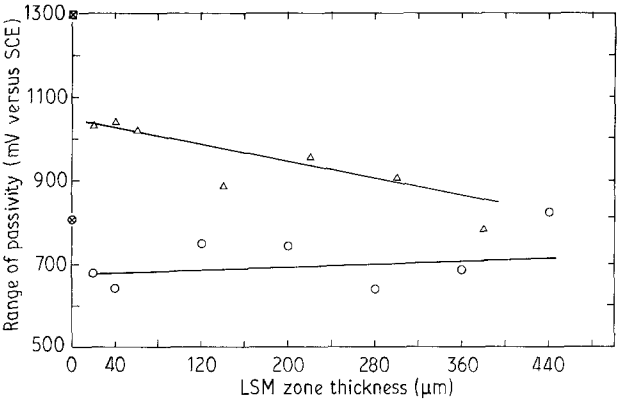

Figure 12 A profile of range of passivity values as a function of LSM zone thickness obtained in 1N H_2SO_4. (⊠) Chromium metal, (⊗) 9Cr–1Mo, (△) ND1, (○) ND2.

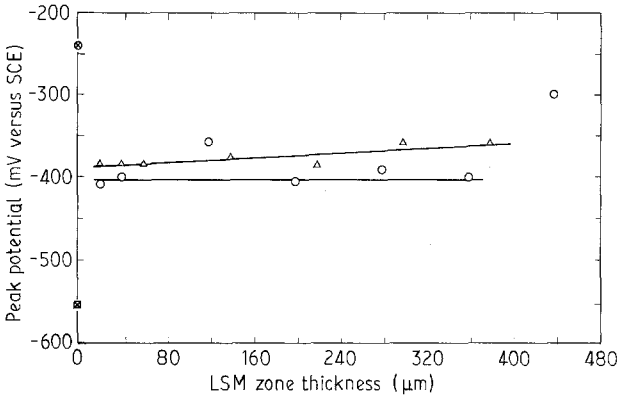

Figure 14 A profile of peak potential values as a function of LSM zone thickness obtained in 1N H_2SO_4. (⊠) Chromium metal, (⊗) 9Cr–1Mo, (△) ND1, (○) ND2.

alloy. On the contrary, specimen ND2 showed much higher values than that of the 9Cr–1Mo alloy which gradually decreased. This indicates that both specimens CO3 and ND2 showed a better range of passivity compared to the 9Cr–1Mo alloy.

3.2.4. Peak potentials and transpassive potentials

Pure chromium metal exhibits a very active peak potential compared to pure iron which shows a less-active peak potential in 1 N H_2SO_4 medium [24]. The addition of chromium to the iron gradually makes the peak potential of such an alloy active towards that of chromium. This fact, though already established, could be observed in Fig. 13, where all three specimens, CO1, CO2 and CO3 show initially very active peak potentials which remain constant up to a certain LSM zone thickness, and then sharply increase. In addition, the peak potentials of all the specimens throughout their LSM zone thickness were found to be very active compared to 9Cr–1Mo alloy. These specimens would be easily passivated in a moderately oxidizing medium. Similar behaviour was also exhibited by specimens ND1 and ND2 (Fig. 14). Specimen ND1 showed almost constant peak potential values throughout the LSM zone, whereas specimen ND2

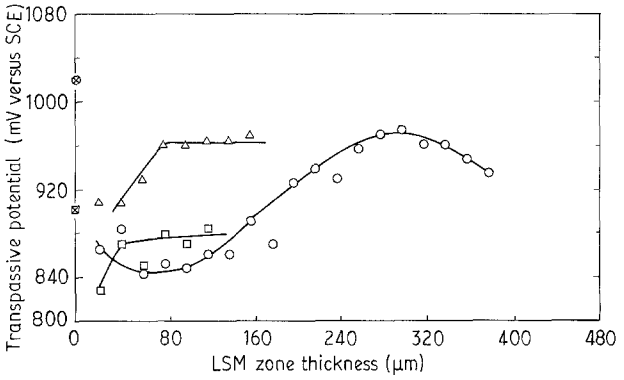

Figure 15 A profile of transpassive potential values as a function of LSM zone thickness obtained in 1N H_2SO_4. (⊠) Chromium metal, (⊗) 9Cr–1Mo alloy, (□) CO1, (○) CO2, (△) CO3.

showed only a slight increase in the values in the LSM zone. Based on these results, we can compare the corrosion behaviour of these laser-treated specimens with that of pure 9Cr–1Mo alloy in this medium. It is already known that the passive film formed over 9Cr–1Mo alloy is not a very protective film because it is made of a loose corrosion product film [16]. The laser-melted surfaces of all these specimens contain much higher chromium concentrations than the base metal. This leads to the fact that these specimens

TABLE V Comparative performance of different specimens

Performance	Passive current density		Peak current density		Range of passivation		Peak potential		Transpassive potential	
	CO2	Nd–YAG	CO2	ND–YAG	CO2	ND–YAG	CO2	ND–YAG	CO2	ND–YAG
Best	CO1		CO3	ND1	CO3	ND1	CO1		CO3	ND1
Better	CO2	ND1	CO1		CO1	ND2	CO2	ND1		ND2
							CO3	ND2		
Fair	CO3	ND2	CO2	ND2	CO2				CO2	
									CO1	

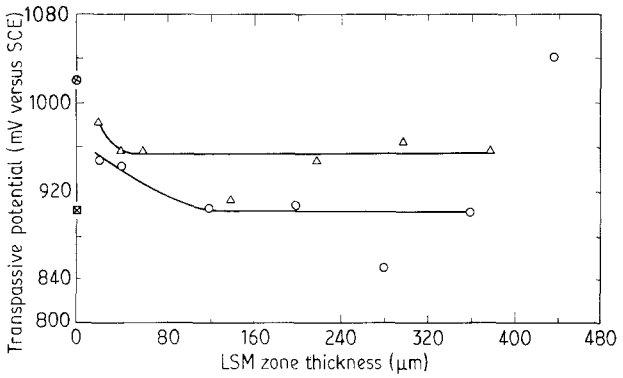

Figure 16 A profile of transpassive potential values as a function of LSM zone thickness obtained in 1N H_2SO_4. (⊠) Chromium metal, (⊗) 9Cr–1Mo, (△) ND1, (○) ND2.

provide a much better corrosion-resistant surface compared to the base metal.

In Figs 15 and 16, the transpassive potentials for CO1, CO2, CO3 and ND1, ND2 have been plotted, respectively, together with that of pure chromium and 9Cr–1Mo alloy. Pure chromium metal shows a low value and the pure iron shows a high value of transpassive potential in 1N H_2SO_4 medium [24]. Addition of chromium to pure iron decreases its transpassive potentials gradually. The plots presented in Fig. 15 for specimens CO1 and CO3 show an initial sharp rise in these values which later become almost constant. However, the initial values for all these specimens were found to be almost equal to or lower than that of even pure chromium metal. The transpassive potential values exhibited by specimens ND1 and ND2 were found to be better or equivalent to pure chromium metal.

Based on the above discussions, different specimens were graded according to their performances with reference to various parameters (Table V). It was found that the overall corrosion resistance in 1N H_2SO_4 medium is improved for specimen ND1 followed by specimens CO1 and CO3. Therefore, the laser parameters and chromium thickness adopted for these specimens could provide an increase in the corrosion resistance of 9Cr–1Mo ferritic steel.

4. Conclusions

The aqueous corrosion resistance of chromium-plated 9Cr–1Mo alloy was studied after laser surface melting by CW CO2 as well as pulsed Nd–YAG laser beams in 1N H_2SO_4 medium. The following conclusions can be drawn on the corrosion resistance of such laser-beam treated specimens.

1. Laser surface melted zone thickness values ranged between 0.1 and 0.5 mm.
2. Passive current density values of the treated surfaces were lower than the 9Cr–1Mo alloy.
3. Peak current density values, as good as pure chromium metal or even better than pure chromium metal, were observed in some specimens.
4. In general, the range of passivity was found to be slightly lower than 9Cr–1Mo alloy, except in the case of specimens CO3 and ND2 which showed an improved range of passivity compared to 9Cr–1Mo alloy.
5. All the specimens showed peak potential values which were much more active compared to 9Cr–1Mo alloy indicating easy passivation characteristics.
6. Transpassive potential values for specimens irradiated by the Nd–YAG laser beam were found to be almost equal to or better than that of pure chromium metal.
7. Laser surface melting could be effectively used to raise the corrosion resistance of the chromium-coated 9Cr–1Mo alloy in 1N H_2SO_4 medium. Specimen ND1, which was laser surface melted by Nd–YAG laser beam, showed the best overall corrosion resistance of all the specimens.

Acknowledgement

The authors thank Shri J. B. Gnanamoorthy, Head, Metallurgy Division, IGCAR, and Dr Placid Rodriguez, Head, Metallurgy and Materials Programme, IGCAR, for their encouragement during the course of above studies. They also thank Dr T. P. S. Gill, Materials Development Division, IGCAR, for his suggestions.

References

1. C. W. DRAPER and J. M. POATE, *Int. Metals Rev.* **30** (1985) 85.
2. S. CHIBA, T. SATO, A. KAWASHIMA, K. ASAMI and K. HASHIMOTO, *Corros. Sci.* **26** (1986) 311.
3. D. S. GNANAMOTHU, in "Applications of Lasers in Materials Processing", edited by E. A. Metzbower (ASM, Cleveland, OH, 1979) p. 177.
4. W. M. STEEN, in "Proceedings of Second European Conference on Laser Treatment of Materials", Bad Nauheim, FRG (1988) p. 60.
5. P. G. MOORE and E. McCAFFERTY, *J. Electrochem. Soc.* **128** (1981) 1391.

6. J. MAZUMDER and J. SINGH, *High Temp. Mater. Proc.* **7** (1986) 101.
7. E. McCAFFERTY, G. K. HUBLER, P. M. HATISHAN, P. G. MOORE, R. K. KANT and B. D. SARTWELL, *Mat. Sci. Engng* **86** (1987) 1.
8. U. KAMACHI MUDALI, R. K. DAYAL, J. B. GANANAMOORTHY, S. M. KANETAKAR and S. B. OGALE, *Mater. Trans. JIM* **33** (1991) 845.
9. U. KAMACHI MUDALI and R. K. DAYAL, *J. Mater. Engng, Perf.* **1** (3) pp. 341–5.
10. N. PARVATHAVARDHINI, R. K. DAYAL, R. SIVAKUMAR, U. KAMACHI MUDALI and A. BHARATHI, *Mater. Sci. Technol.*, in press.
11. T. R. ANTHONY and H. E. CLINE, *J. Appl. Phys.* **49** (1978) 1248.
12. J. STEWART, D. B. WELLS, P. M. SCOTT and A. S. BRANSDEN, *Corrosion* **46** (1990) 618.
13. J. C. ION, T. MOISIO, T. F. PEDERSON, B. SORENSEN and C. M. HANSSON, *J. Mater. Sci.* **26** (1991) 43.
14. W. J. TOMLINSON and M. G. TALKS, *ibid.* **26** (1991) 804.
15. R. P. SINGH, O. P. MODI, M. N. MUNGOLE and R. P. SINGH, *Brit. Corros. J.* **20** (1985) 28.
16. N. PARVATHAVARDHINI, R. K. DAYAL and J. B. GNANAMOORTHY, *Bull. Electrochem.* **6** (1990) 20.
17. M. G. PUJAR and R. K. DAYAL, in "Proceedings of the International Symposium on Industrial Metal Finishing", Karaikudi, India (1989).
18. P. G. MOORE, in Proceedings of the International Symposium on "Fundamental Aspects of Corrosion Protection by Surface Modification", edited by E. McCafferty, C. E. Clayton and J. Oudar (The Electrochemical Society, 1984) p. 102.
19. Micheal Bass (ed.), "Laser Materials Processing: Materials Processing–Theory and Practice", Vol. 3 (North Holland, Amsterdam, 1983) p. 239.
20. G. MOULIN, J. M. SIFFRE and P. MARCUS, *Mater. Sci. Technol.* **6** (1990) 100.
21. G. MOULIN, *J. Mater. Sci.* **26** (1991) 756.
22. P. T. COTTRELL, R. P. FRANKENTAL, G. W. KAMMLOTT and D. J. SICANOLFI and C. W. DRAPER, *J. Electrochem. Soc.* **130** (1983) 998.
23. H. J. HEGGE, J. TH. M. DE HOSSON, *J. Mater. Sci.* **26** (1991) 711.
24. M. G. Fontana and R. W. Staehle (eds), "Advances in Corrosion Science and Technology," Vol. 3 (Plenum Press, New York, 1973) p. 309.

Received 28 May
and accepted 29 October 1992